

A Super Bubble Candidate in the Galactic Center and a Local Enhancement G 359.77–0.09

Hideyuki MORI,^{1,2} Yoshiaki HYODO,¹ Takeshi Go TSURU,¹ Masayoshi NOBUKAWA,¹ and Katsuji KOYAMA,¹

¹*Department of Physics, Graduate School of Science, Kyoto University, Sakyo-ku, Kyoto, 606-8502*

²*Department of High Energy Astrophysics, Institute of Space and Astronautical Science (ISAS), Japan Aerospace Exploration Agency (JAXA),
3-1-1, Yoshinodai, Sagamihara, Kanagawa, 229-8510
mori@astro.isas.jaxa.jp*

(Received (reception date); accepted (acceptation date))

Abstract

A $20' \times 16'$ elliptical ring-like structure has been found near the Galactic center in the narrow energy band corresponding to the $K\alpha$ line from He-like sulfur. In the ring, two diffuse sources are found, a supernova remnant candidate G 359.79–0.26 and an unidentified source G 359.77–0.09. The X-ray spectrum of G 359.77–0.09 is similar to that of G 359.79–0.26, which can be explained by an absorbed thin thermal plasma model with temperatures of 0.7 and 1.0 keV. The absorption column densities of these two sources are large ($N_{\text{H}} = 6.9 \times 10^{22}$ and $4.5 \times 10^{22} \text{ cm}^{-2}$) and are consistent with that of the Galactic center distance. The X-ray spectrum extracted from the ring-like structure is also represented by an absorbed thin thermal plasma model ($kT_{\text{e}} \sim 0.9 \text{ keV}$). The thermal energy of the plasma filling the ring-like structure is estimated to be $1.0 \times 10^{51} \text{ erg}$. We therefore propose that the two sources comprise a single ring-like object, which is possibly a super bubble with a size of $49 \text{ pc} \times 40 \text{ pc}$ in the Galactic center region.

Key words: Galaxy: center₁ — ISM: individual (G 359.77–0.09)₂ — ISM: supernova remnants₃ — X-rays: ISM₄

1. Introduction

Super bubbles (SBs) are large-scale diffuse objects in galaxies heated by shocks of sequential supernova (SN) explosions and/or strong stellar winds from a number of massive stars. The temperature of the shock-heated gas reaches 10^{6-7} K so that SBs emit diffuse soft X-rays. The most complete and measurable samples of the X-ray SBs are those in the Large Magellanic Cloud (LMC). Dunne et al. (2001) surveyed the X-ray SBs in the LMC with the ROSAT satellite and reported X-ray emission from 13 SBs. However, no detailed spectral information was available due to limited photon statistics. The XMM-Newton satellite re-visited some of these SBs and found their temperatures to be typically 0.1–0.2 keV, similar to those of old supernova remnants (SNRs, e.g., Nazé et al. 2004). One exception is 30 Dor C where some parts of the SB show hard spectra with a power-law index of 2.7 (Bamba et al. 2004). The follow-up observation with Suzaku found that the hard emission is not a single power-law but can be described either by a model of a broken power-law or synchrotron radiation (Yamaguchi et al. 2009), indicating the presence of non-thermal X-ray emission due to shock-accelerated electrons.

In our Galaxy, the X-ray study of SBs has been limited. This may be due to their possible soft X-ray spectra, so that most of the SBs, if any, are invisible because of the large absorption through the Galactic plane. Diffuse X-rays from the Cygnus super bubble (e.g., Cash et al. 1980), Orion-Eridanus (Guo et al. 1995), Gemini-Monoceros (Plucinsky et al. 1996), and possibly the North Polar Spur (e.g., Egger & Aschenbach 1995) are a few examples of the Galactic SB candidates. The spectra of these sources are all soft with a plasma temperature around

0.1–0.3 keV. These would be near-by objects, because of their low absorption ($N_{\text{H}} \sim (1-10) \times 10^{20} \text{ cm}^{-2}$), their positions at high Galactic latitude, and the apparent large ($\sim 25^\circ \times 25^\circ$) angular sizes. However the real distances of these sources are very uncertain, and hence many important physical parameters such as the physical size, the total luminosity, and the density of these SBs are not determined well. Furthermore these form a very limited and biased sample of the Galactic SBs, because the majority should be prevailing in sites of massive star formation which mainly reside in the Galactic plane.

If a sizeable number of the SBs in our Galaxy have higher temperatures and/or hard components, we may be able to detect these SBs by X-rays. The Galactic center (GC) is a good region for this study since the distance is well known. The purpose of this paper is to search for SB candidates in the GC and to study their physical properties.

In this paper, we briefly explain our GC observation with Suzaku (Mitsuda et al. 2007) and the data reduction in section 2. The results of the imaging and spectral analyses are described in section 3. We then discuss a new SB candidate in the GC, together with the physical properties of the bright X-ray clump, in section 4. A summary is given in section 5. Throughout this paper, the quoted errors represent the 90% confidence limits, unless otherwise mentioned. We also adopt Galactic coordinates in which the north and east are defined to be the positive Galactic latitude and longitude, respectively.

2. Observation and Data Reduction

The X-ray CCD cameras (X-ray Imaging Spectrometer, XIS; Koyama et al. 2007a) on board Suzaku, combined with the X-

Table 1. Observation log of the GC regions

Target	SCI	Obs. ID	Start time (UT)	End time (UT)	Exposure*
Sgr A East	off	100027010	2005-09-23T07:18:25	2005-09-24T11:05:19	45 ks
		100037040	2005-09-30T07:43:01	2005-10-01T06:21:24	43 ks
Sgr A West	off	100027020	2005-09-24T14:17:17	2005-09-25T17:27:19	43 ks
		100037010	2005-09-29T04:35:41	2005-09-30T04:29:19	44 ks
GC South	on	501008010	2006-09-26T14:18:16	2006-09-29T21:25:14	142 ks
GC South BGD	on	501009010	2006-09-29T21:26:07	2006-10-01T06:55:29	56 ks

* Effective exposure of the screened XIS data

Ray Telescopes (XRTs; Serlemitsos et al. 2007), provide excellent imaging spectroscopy capabilities. In particular, given the low background of the XIS and the high throughput of the XRTs, Suzaku is suitable for detecting the diffuse X-ray emission with low surface brightness.

Suzaku observed the Sgr A East region and its western region (hereafter Sgr A West) twice on 2005 September, during the Performance Verification phase (Koyama et al. 2007c). The southern and northern regions, referred to as GC South and GC South BGD hereafter, were subsequently observed on 2006 September (in the AO-1 cycle) for the purpose of mapping the GC. The XIS was operated with the normal clocking and the full window modes (Koyama et al. 2007a) in all of the observations. Furthermore, in the last two observations, the Spaced-row Charge Injection (SCI; Bautz et al. 2004, Nakajima et al. 2008) was applied to improve the time-degraded energy resolution. The observation log is summarized in table 1.

We analyzed the XIS data using the processing version of 2.0.6.13¹. In this processing, the energy scale of the XIS data is calibrated to within 10 eV at 6 keV, irrespective of applying the SCI (Uchiyama et al. 2007). We followed the standard criteria as recommended by the Suzaku XIS team² for screening the XIS data. We first filtered out the data during the times of passage of South Atlantic Anomaly and of low cut-off rigidity (< 6 GV). We then used the data taken with the Earth rim angles of $< 5^\circ$ and the sun-lit Earth rim angles of $< 20^\circ$. Hot and flickering pixels were removed with `cleansis v1.7`. Finally, we combined the events taken in the 3×3 and 5×5 editing modes with `XSELECT v2.3`. The effective exposure times of the four regions are 88 ks (Sgr A East), 87 ks (Sgr A West), 142 ks (GC South), and 56 ks (GC South BGD), respectively.

Using these data sets, we searched SB candidates as described in the following sections. We created the XIS images and spectra with `XSELECT v2.3`. The spectral analyses were carried out using `XSPEC v11.3.2`. The Redistribution Matrix File (RMF) and Auxiliary Response File (ARF) were made via `xisrmfgen` and `xissimarfgen` (Ishisaki et al. 2007), respectively, which are provided through the Suzaku FTOOLS in HEASOFT v6.4. We used the XIS CALDB 20080709 to construct the RMF and ARF.

3. Analysis

The XIS mosaic images in the $K\alpha$ -line bands of He-like sulfur (2.35–2.55 keV) and He-like iron (6.6–6.75 keV) are shown

in figure 1. The images extracted from the respective observations were summed together and were binned by a factor of 8 (1 pixel = $1''.04 \times 1''.04$) followed by smoothing with the Gaussian kernel of $\sigma = 1.4$. We applied the exposure correction to the images, which includes the vignetting effect of the XRTs.

The image of the $K\alpha$ line from He-like sulfur traces the spatial distribution of a thermal plasma with the temperature of $\sim 10^7$ K. On the other hand, that from He-like iron indicates the spatial distribution of the Galactic Center Diffuse X-rays (GCDX; Koyama et al. 1989).

In the $K\alpha$ -line band image of He-like sulfur (figure 1a), there are some bright regions which are positionally coincident with Sgr A East (Maeda et al. 2002), G 359.79–0.26, and G 359.77–0.09; the latter two clumps are designated by Senda et al. (2003). Furthermore, we can see an elliptical ring connecting these diffuse X-ray emission.

On the other hand, the $K\alpha$ -line band image of He-like iron (figure 1b) shows no ring structure. Sgr A East is by far brightest source; its surface brightness of $> 5 \times 10^{-3}$ cts s^{-1} arcmin $^{-2}$ (blue region in figure 1b) is an order of magnitude larger than those of G 359.79–0.26 and G 359.77–0.09 ($\sim 5 \times 10^{-4}$ cts s^{-1} arcmin $^{-2}$). The surface brightness of the inside region of the ring is the same as those of the two clumps. Hence, the absence of the ring structure in figure 1b is not caused by any color contrast effects. Furthermore, since the ratio of the surface brightness of Sgr A East ($\sim 4 \times 10^{-4}$ cts s^{-1} arcmin $^{-2}$) to that of G 359.79–0.26 ($\sim 1 \times 10^{-4}$ cts s^{-1} arcmin $^{-2}$) is at most 4 in the $K\alpha$ -line band of He-like sulfur, the additive higher-temperature plasma probably exists towards Sgr A East; Koyama et al. (2007b) indicated the presence of the 6 keV ($\sim 7 \times 10^7$ K) plasma by the spectral analysis of Sgr A East. Therefore it may be possible that there is a ring structure composed of the $\sim 10^7$ K temperature plasma and Sgr A East is unrelated to this object.

For the two bright regions in the ring structure of figure 1a, the spectral analysis of SNR G 359.79–0.26 has been already carried out by Mori et al. (2008). Senda et al. (2003) reported that G 359.77–0.09 shows a thermal spectrum with the plasma temperature of ~ 1 keV. However, its origin is not clear. We therefore first generated and analyzed the X-ray spectrum of G 359.77–0.09 in section 3.1. We describe a more quantitative analysis of the ring structure in section 3.2 and 3.3.

3.1. G 359.77–0.09

We extracted the source spectrum from the elliptical region shown in figure 1a. The center of the source region is $(l, b) = (+359^\circ 7751, -0^\circ 0623)$. The semi-major and semi-

¹ <http://www.astro.isas.jaxa.jp/suzaku/process/history/v20613.html>

² http://www.astro.isas.jaxa.jp/suzaku/process/v2changes/criteria_xis.html

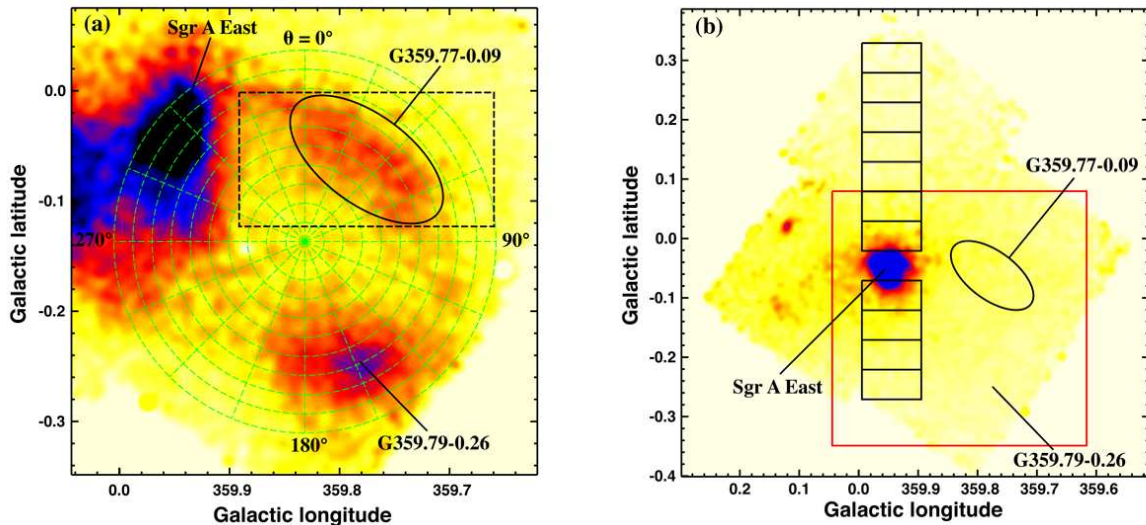


Fig. 1. XIS mosaic images of the GC region in the $K\alpha$ -line bands of He-like sulfur (a; 2.35–2.55 keV) and He-like iron (b; 6.6–6.75 keV). Both images were binned by 8×8 pixels and then were smoothed with $\sigma = 1.4$. The exposure time and the vignetting effect of the XRTs were corrected. The field of view of the $K\alpha$ -line band image of He-like sulfur is indicated by a red solid square in that of He-like iron. The regions used to extract the G 359.77–0.09 and its background spectra are drawn by a solid ellipse and a dashed rectangle, respectively, in the $K\alpha$ -line band image of He-like sulfur. A green dotted “spider web” and a series of rectangles were used to investigate the radial surface brightness profiles (see section 3.2) and the flux distribution along the Galactic latitude (see section 3.1.1), respectively.

minor axes of the region are 4.9 and 2.4 , respectively. We selected the periphery of the source region as a local background region (the dashed rectangle excluding the source region in figure 1a).

We first subtracted the non X-ray background (NXB; Tawa et al. 2008) from the source and local background spectra and then calculated the effective areas for the source and background regions with `xissimarfgen` in order to investigate the difference of the energy-dependent telescope vignetting. We then applied the vignetting correction to the background spectra. Finally, the G 359.77–0.09 spectrum was made by subtracting the vignetting-corrected background spectrum. The background-subtracted spectrum is shown in figure 2, which clearly shows the $K\alpha$ lines from the He-like ions of Si, S, and Ar, while the Ca- and Fe- $K\alpha$ lines are marginal.

We fitted the spectrum with a thin thermal plasma model in collisional ionization equilibrium (CIE) absorbed by photoelectric absorption with the cross sections given in Balucinska-Church & McCammon (1992). The elemental abundances of Si, S, and Ar were free parameters. The plasma temperature of $kT_e = 0.66$ keV and the solar abundances gave an acceptable fit ($\chi^2 = 73/100$ d.o.f.). The absorption column density is $N_H = 6.9 \times 10^{22}$ cm $^{-2}$. The best-fit parameters are summarized in table 2. The best-fit model is given with the solid line in figure 2. We note that we tried to fit the spectrum with a non-equilibrium ionization plasma model instead of the CIE plasma model. The best-fit parameter of the ionization timescale (n_{et}) is $8.0^{+490}_{-4.6} \times 10^{11}$ cm $^{-3}$ s. Moreover, those of the temperature ($kT_e = 0.72$ keV) and absorption ($N_H = 6.3 \times 10^{22}$ cm $^{-2}$) are consistent with those obtained with the CIE plasma model. Thus, we adopt the best-fit parameters of the CIE plasma in the following discussion.

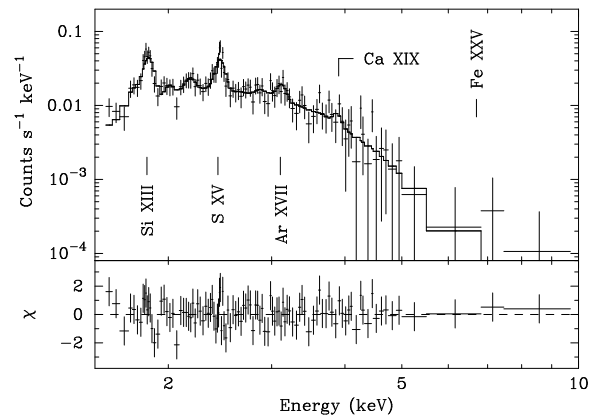


Fig. 2. Background-subtracted spectrum of G 359.77–0.09. The solid line represents the best-fit thin thermal plasma model.

3.1.1. Spatial distribution of the GCDX emission

The GCDXs are the most serious source of local background for G 359.77–0.09, because the GCDX flux is position-dependent (Koyama et al. 2007c) and G 359.77–0.09 is a faint diffuse source located near the GC on the Galactic plane ($b = -0.05$). We therefore checked whether or not the GCDX subtraction was done properly.

The $K\alpha$ line from He-like iron (6.7 keV) is a good indicator of the GCDX emission (see figure 1b). The 6.7 keV line fluxes along the Galactic longitude are available from Koyama et al. (2007c), so that we examined the 6.7 keV line fluxes along the Galactic latitude.

We extracted spectra in the 5.5–11.5 keV band from a series

Table 2. Best-fit parameters of the G 359.77–0.09 and the GC ring spectra*

Parameters	Values		
	G 359.77–0.09	GC ring	GC faint ring
N_{H} (10^{22} cm $^{-2}$)	6.9 (6.1–7.6)	5.5 (5.2–5.7)	5.5 (5.0–6.0)
kT_{e} (keV)	0.66 (0.57–0.74)	0.91 (0.88–0.94)	0.96 (0.88–1.07)
Z_{Si}^{\dagger}	0.9 (0.7–1.3)	1.0 (0.9–1.2)	0.9 (0.6–1.2)
Z_{S}^{\dagger}	0.7 (0.6–1.0)	1.2 (1.1–1.3)	1.3 (1.0–1.6)
Z_{Ar}^{\dagger}	0.9 (0.3–1.7)	1.4 (1.1–1.7)	1.6 (1.0–2.2)
Normalization ‡	0.08 (0.05–0.14)	0.06 (0.05–0.07)	0.016 (0.012–0.022)
Flux (1.5–5 keV) §	3.0×10^{-4}	7.2×10^{-4}	2.2×10^{-4}
$\chi^2/\text{d.o.f.}$	73/100 = 0.73	143/152 = 0.94	62/98 = 0.63

* The values in parentheses represent the 90% confidence intervals.

† Elemental abundances relative to solar.

‡ In unit of $10^{-14}/(4\pi D^2) \int n_{\text{e}} n_{\text{H}} dV$ cm $^{-5}$. Here V and D are the volume and distance to the plasma, respectively.

§ Absorbed flux in units of photons s $^{-1}$ cm $^{-2}$.

of $6' \times 3'$ rectangular regions in figure 1b. We fixed the central longitude of each rectangle to be $l = +359^{\circ}9443$, the same Galactic longitude as that of Sgr A*. After the NXB subtraction, each spectrum was fitted by the same phenomenological model as that used in Koyama et al. (2007c); an absorbed thermal bremsstrahlung with several Gaussian emission lines.

We plot the best-fit parameters of the 6.7 keV line fluxes along the Galactic latitude in figure 3. Although the flux distribution is highly asymmetric along the Galactic longitude with respect to the Galactic center (Koyama et al. 2007c), that along the Galactic latitude at $l = +359^{\circ}9443$ is roughly symmetric with respect to the Galactic plane. The 6.7 keV line fluxes are decreased exponentially with the distance from the Sgr A*, except for the direction along the Galactic positive longitude. We therefore fitted the 6.7 keV line fluxes along the Galactic negative longitude and latitude (both positive and negative latitudes) simultaneously with an exponential model given by,

$$F(l, b) = A \exp\left(-\frac{|l - l_c|}{\sigma_l} - \frac{|b - b_c|}{\sigma_b}\right), \quad (1)$$

where l_c and b_c are fixed to the position of Sgr A*. We obtained the best-fit parameters as follows; $A = (3.5 \pm 0.2) \times 10^{-6}$ photons s $^{-1}$ cm $^{-2}$ arcmin $^{-2}$, $\sigma_l = 0^{\circ}22 \pm 0^{\circ}02$, and $\sigma_b = 0^{\circ}14 \pm 0^{\circ}01$. We show the best-fit model at $l = +359^{\circ}9443$ with a black dashed line in figure 3.

Assuming the validity of equation 1 in the GC region, we inferred the 6.7 keV flux distribution at the G 359.77–0.09 position ($l = +359^{\circ}7751$), as is indicated by a red dashed line in figure 3. The estimated flux at G 359.77–0.09 ($l = +359^{\circ}7751$, $b = -0^{\circ}0623$) is 1.43×10^{-6} photons s $^{-1}$ cm $^{-2}$ arcmin $^{-2}$.

On the other hand, we fitted the NXB-subtracted source spectrum (X-ray background unsubtracted G 359.77–0.09 spectrum) with an absorbed thermal bremsstrahlung plus several Gaussian emission lines. We obtained the best-fit 6.7 keV line flux to be $(1.36 \pm 0.07) \times 10^{-6}$ photons s $^{-1}$ cm $^{-2}$ arcmin $^{-2}$, as is indicated by a red circle in figure 3, and it is consistent with the model estimation. This consistency indicates that the 6.7 keV line flux in the source region can be attributed to the GCDX emission. Thus no flux at the 6.7 keV line in the G 359.77–0.09 spectrum (see figure 2) supports that our GCDX subtraction was done accurately.

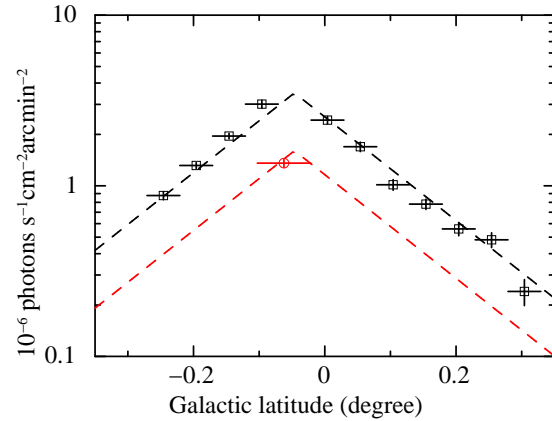


Fig. 3. The 6.7 keV line fluxes of G 359.77–0.09 (red circle) and the ladder area along the Galactic latitude (black squares). The black and red dotted lines represent the best-fit models of the flux distribution along the Galactic latitude at $l = +359^{\circ}9443$ and $l = +359^{\circ}7751$, respectively.

3.2. Large-scale ring structure

To verify the presence of the ring structure quantitatively, we constructed the radial surface brightness profile from the $K\alpha$ -line band image of He-like sulfur. We divided a circular region centered at $(l, b) = (+359^{\circ}8312, -0^{\circ}1367)$ into 10 annuli, each of which has a radial width of $1'$, and separated the respective annuli into 16 sectors with an azimuthal angle of $22^{\circ}5$. We show these sectors with a green dotted spider web in figure 1a.

The radial profiles in the 12 directions are shown in figure 4. The uppermost profile corresponds to the north-northeast direction ($\theta = 337^{\circ}5-0^{\circ}0$ in figure 1a), and the profiles in the other directions are placed from top to bottom in the clockwise order. We ignored the 4 sectors from the east-eastsouth to the north-northeast, where the contamination from Sgr A East is significant because of the $\sim 2'$ angular resolution of the XRTs.

We connect the brightness peak of each profile (indicated by arrows) with a smooth dashed line. Since the peak positions are in the range of $5'.7-7'.8$ and comprise an S-shaped line, we

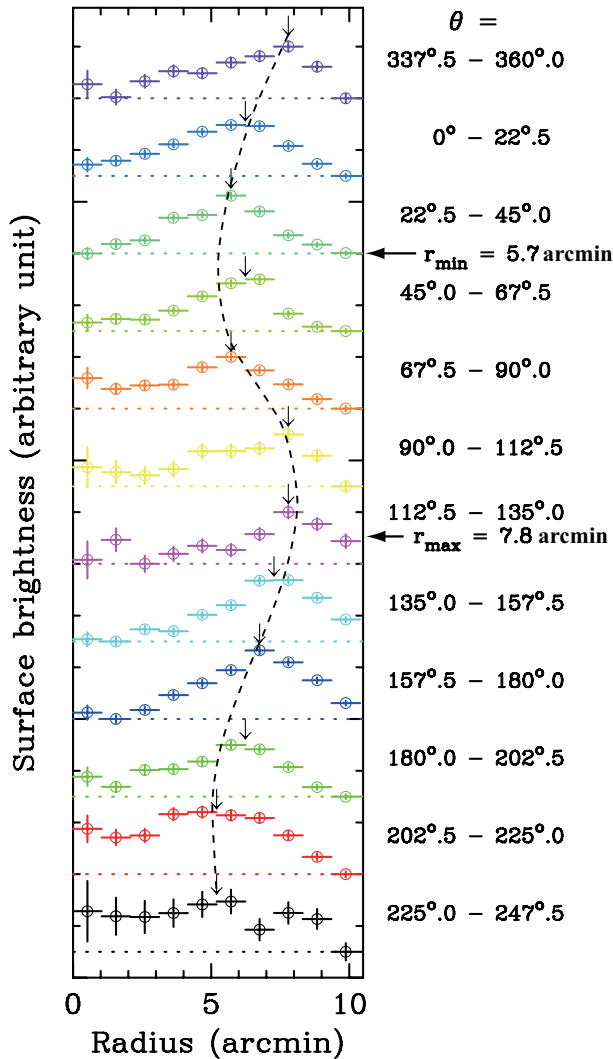


Fig. 4. Radial surface brightness profiles in the 12 azimuthal directions. The error bars represent the 1σ confidence limits. For clarity, the vertical axis of each profile is scaled arbitrarily. The background level of each profile is represented by a dotted line. The profiles are shown in clockwise order from the north-northeast direction (top) to the east-east south direction (bottom). The azimuthal angle of each profile (north is $\theta = 0^\circ$ and west is $\theta = 90^\circ$; see figure 1a) is given in the right side of the panel. To guide the eye, we show a sinusoidal line (dashed line) approximately following the brightness peak in each direction (indicated by arrows).

suggest that there is a large elliptical ring toward the GC. Since each profile has a width of $6' - 9'$ around the peak, the size of the outer boundary of the ring is estimated to be $\sim 20' \times 16'$.

We next made a GC image consisting of the $K\alpha$ emission from He-like sulfur. We created the narrow-band images in 2.39–2.52 (hereafter image A), 1.9–2.3 (image B), and 2.6–3.0 keV (image C) for each observation. The images in the latter two energy bands are used to estimate the continuum component in the 2.39–2.52 keV band. These images were binned by $32 \text{ pixel} \times 32 \text{ pixel}$ ($0'.55 \times 0'.55$) and summed to make the GC mosaic images. After the scaling of the image-extraction energy ranges, we subtracted the image B and C from the image A. The continuum-subtracted GC image was corrected for the exposure and vignetting effects and then smoothed with the Gaussian of $\sigma = 1'.66$. The $K\alpha$ line image of He-like sulfur is shown in figure 5a.

The image again shows a ring-like structure; the surface brightness of the connecting region between G 359.77–0.09 and G 359.26–0.79 and that between G 359.26–0.79 and Sgr A East is ~ 2 times larger than that of the inside region of the ring. Furthermore, we investigated the significance of detecting the $K\alpha$ emission from He-like sulfur. Assuming that each $32 \text{ pixel} \times 32 \text{ pixel}$ ($0'.55 \times 0'.55$) area contains X-ray photons of C_A for the image A, C_B for the image B, and C_C for the image C, the significance level (S/N ratio) is calculated by $(C_A - C_B f_B - C_C f_C) / \sqrt{C_A + C_B f_B^2 + C_C f_C^2}$, where f_B and f_C are the scaling factors due to the image-extraction energy ranges. The S/N ratio inside the ring (indicated by yellow color in figure 5a) region is $1.5 - 2\sigma$ in each unit area ($32 \text{ pixel} \times 32 \text{ pixel}$), while that on the ring region (indicated by orange color) is about $2.5 - 3\sigma$.

We also made a GC image due to the $K\alpha$ emission from He-like and H-like iron (see figure 5b). Here we selected the energy bands of 6.5–7.0 keV (image A), 4.5–6.0 keV (image B), and 7.2–8.0 keV (image C). The image was made by the same method as that of the $K\alpha$ emission from He-like sulfur. As is shown in figure 1b, we can see that there is the strong emission centered at Sgr A East and that the ring structure in figure 5a is absent.

3.3. The Ring Spectra

We extracted a spectrum from the elliptical arc-like region encircled with solid curves in figure 5a. We removed a part of the ring structure (hereafter GC ring) where the contamination from Sgr A East cannot be negligible from the source-extraction region. The sizes of the outer and inner elliptical arcs are $20' \times 16'$ and $8'.0 \times 6'.4$, respectively. The background region is drawn by a dashed polygon excluding the source-extraction region. We also added the inside of the GC ring (indicated by an ellipse with a red slash) to the background region.

The GC-ring spectra were extracted from the GC South and Sgr A West observations, while the background spectra are done from the GC South, GC South BGD, and Sgr A West observations. We created the corresponding NXB spectra by `xisnxbgen` which were subtracted from the ring and background spectra. For all the spectra the energy-dependent vignetting corrections described in section 3.1 were applied. The ring and background spectra were normalized by the effective

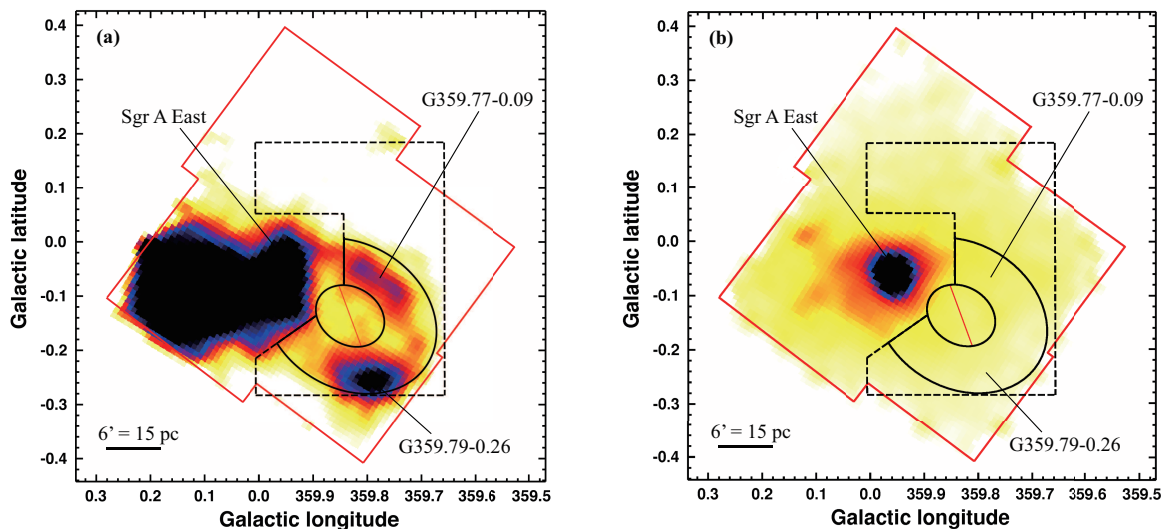


Fig. 5. GC mosaic images of He-like sulfur $K\alpha$ -line (a), and He-like and H-like iron $K\alpha$ -lines (b). The images were binned by 32×32 pixels and the continuum fluxes were then subtracted (see text) and the images were smoothed with $\sigma = 1.66$. The exposure time and the vignetting effect of the XRTs were corrected. The XIS field of view is indicated by a red polygon. The GC-ring spectrum is extracted from the elliptical arc-like region encircled with solid curves. The background region is shown by a dashed polygon excluding the source-extraction region and an ellipse with a red slash.

area and were summed together. Finally, we subtracted the background spectrum from the ring spectrum, which is shown in figure 6a.

The spectrum clearly shows the Si, S, and Ar emission lines, in addition to a marginal emission line due to He-like Ca. We fitted the spectrum by an absorbed CIE plasma model with the variable abundances of Si, S, and Ar. The best-fit parameters of the absorption column density and the electron temperature are $N_{\text{H}} = 5.5 \times 10^{22} \text{ cm}^{-2}$ and $kT_e = 0.91 \text{ keV}$. The elemental abundances of Si, S, and Ar are solar or subsolar values. The results are summarized in table 2. We note that all the best-fit parameters of the absorption column density, the electron temperature, and the elemental abundances are intermediate values between those of G 359.77–0.09 (see section 3.1) and G 359.79–0.26 (see table 3 of Mori et al. 2008).

Furthermore, we made a ring spectrum excluding the G 359.77–0.09 and G 359.79–0.26 emission to examine whether the region with the faint $K\alpha$ -line emission from He-like sulfur (referred as to faint ring hereafter) is related to these two bright clumps. The excluded regions for G 359.77–0.09 and G 359.79–0.26 are the same as that described in section 3.1 (see also the solid ellipse in figure 1a) and that described in section 3 of Mori et al. (2008), respectively. As is shown in figure 5b, the periphery of G 359.77–0.09 shows relatively bright $K\alpha$ -line emission from highly ionized iron because of its location. Thus, in order to extract the corresponding background spectrum, we removed the area overlapped with the dashed rectangle shown in figure 1a from the background region. We again subtracted the background spectrum after applying the vignetting correction. The X-ray spectrum of the faint ring is shown in figure 6b.

The spectrum shows the $K\alpha$ emission lines from He-like Si, S, and Ar. This feature is similar to that of the ring spec-

trum shown in figure 6a, and indicates that the X-ray emission has a thin thermal plasma origin. We fitted the faint ring spectrum with an absorbed CIE plasma model. The elemental abundances of Si, S, and Ar were allowed to vary again. The best-fit parameters are consistent with those derived from the ring spectrum including the G 359.77–0.09 and G 359.79–0.26 emission; the X-ray emission from the plasma with the temperature of $kT_e = 0.96 \text{ keV}$ is attenuated with the absorption of $N_{\text{H}} = 5.5 \times 10^{22} \text{ cm}^{-2}$. We summarized the best-fit parameters in table 2. This result strengthens the physical connection of the faint ring emission to G 359.77–0.09 and G 359.79–0.26.

4. Discussion

4.1. G 359.77–0.09

The X-ray spectrum of G 359.77–0.09 clearly shows the presence of a thin thermal plasma ($kT_e \sim 0.7 \text{ keV}$). The heavy absorption of $N_{\text{H}} = 6.9 \times 10^{22} \text{ cm}^{-2}$ indicates that the plasma is located in the GC. Using the best-fit plasma parameters derived from the G 359.77–0.09 spectral analysis, we can estimate some physical properties. Assuming that the distance to the plasma is 8.5 kpc, the emission measure is estimated to be $6.9 \times 10^{58} \text{ cm}^{-3}$. If the plasma is an ellipsoid with the dimensions of $4.9 \times 2.4 \times 2.4$, corresponding to $12 \text{ pc} \times 6.0 \text{ pc} \times 6.0 \text{ pc}$ in the GC, the volume of the X-ray emitting plasma is $3.9 \times 10^{58} \text{ cm}^3$. The electron density of the plasma is then derived to be $1.3f^{-1/2} \text{ cm}^{-3}$, where f is a filling factor.

The elemental abundances of the plasma are consistent with the solar values, which implies that the X-ray emitting plasma has an interstellar medium (ISM) origin. The total mass of the plasma is $M = 1.4n_e m_p V = 58f^{1/2} M_{\odot}$ (m_p represents the proton mass), and its thermal energy is estimated to be

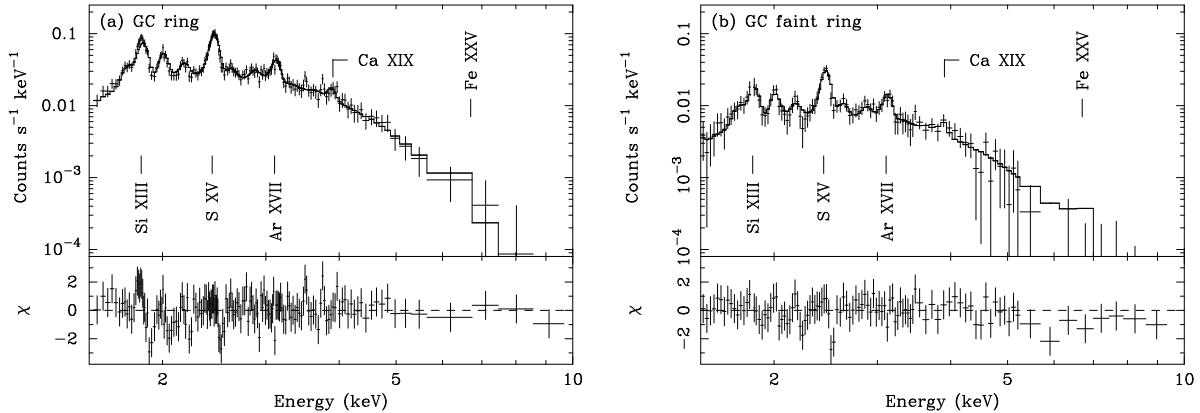


Fig. 6. Background-subtracted spectra of the GC ring (a) and the GC faint ring (b). The solid line represents the best-fit thin thermal plasma model.

$E_{\text{th}} = \frac{3}{2} \frac{MkT_e}{\mu m_p} = 1.9f^{1/2} \times 10^{50}$ erg. Here μ represents the mean atomic weight of 0.604. The plasma temperature gives the sound speed of $v_s = (kT_e\gamma/\mu m_p)^{1/2} \simeq 430$ km s $^{-1}$, when assuming the energy equipartition of electrons and ions. γ represents the specific heat ratio of 5/3. By dividing the semi-major axis of the plasma (4.9 ~ 12 pc) by its velocity, we can estimate the dynamical age of the plasma to be $t_{\text{dyn}} = 2.7 \times 10^4$ yr.

The thermal energies of G 359.77–0.09 and G 359.79–0.26 are similar to each other (1.9×10^{50} erg and 1.7×10^{50} erg, respectively), although the apparent X-ray flux of the former is 1.7 times smaller than that of the latter. This difference comes from the different plasma densities. Therefore the X-ray fainter ring regions other than the two spots may have comparable thermal energies.

4.2. Super bubble

The radial profile indicates that the brightness peaks comprise an elliptical ring at the center of $(l, b) = (+359^\circ 8312, -0^\circ 1367)$. The X-ray spectrum of G 359.77–0.09, which is on the elliptical annular structure, is similar to that of G 359.79–0.26, another bright spot on the elliptical annulus, while the absorption of $N_{\text{H}} = 6.9 \times 10^{22}$ cm $^{-2}$ is 1.5 times larger than that of G 359.79–0.26 ($N_{\text{H}} = 4.5 \times 10^{22}$ cm $^{-2}$).

We therefore examined the N_{H} dependence on the Galactic latitude near to G 359.77–0.09 and G 359.79–0.26 using the GCDX spectra in the ladder of figure 1b, because this ladder region is free from the two sources. The best-fit column densities (N_{H}) are shown in figure 7, where the arrows show the latitudes of the two sources.

Using figure 7, the N_{H} ratio at the center latitudes of the two sources is estimated to be $7.6/5.0 = 1.5$, exactly the same as that calculated by the observed N_{H} ($6.9/4.5 = 1.5$). Thus we can infer that both G 359.77–0.09 and G 359.79–0.26 are located at the same distance, the GC region, and that these two bright spots are physically associated.

The elliptical annular structure has an apparent size of $20' \times 16'$, which corresponds to 49 pc \times 40 pc at the distance of 8.5 kpc. While the spatial extent is half of a typical size of the SBs (~ 100 pc, for instance, the physical size of the Orion-

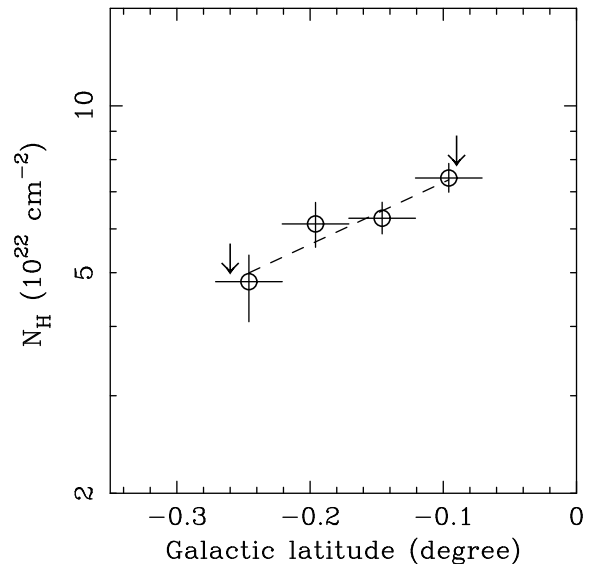


Fig. 7. Best-fit N_{H} parameters in the ladder region of figure 1b in the Galactic negative latitude. The dashed line is drawn to guide the eye and the arrows show the latitude positions of G 359.77–0.09 and G 359.79–0.26.

Eridanus SB is 80 pc \times 160 pc given its distance of 226 pc; see Guo et al. 1995), it is 4–5 times larger than that of the nearest GC SNR, Sgr A East (~ 10 pc; Maeda et al. 2002).

We generated a GC-ring spectrum which averages the spectra of G 359.77–0.09, G 359.79–0.26, and the connecting region, and then derived a heavy absorption column of $N_{\text{H}} = 5.5 \times 10^{22}$ cm $^{-2}$ and a plasma temperature of $kT_e = 0.91$ keV. Owing to the good photon statistics, we can determine the emission measure precisely, which is calculated to be 5.2×10^{58} cm $^{-3}$ at the GC distance. The volume of the GC ring (i.e., the elliptical arc-like region in figure 5) is estimated to be 7.6×10^{59} cm 3 if the dimension along the line of sight is equal to that of the semi-minor axis. The electron density and mass of the plasma are then found to be $0.26f^{-1/2}$ cm $^{-3}$ and $232f^{1/2}M_{\odot}$, respectively, where f again represents a filling

factor. Consequently, the thermal energy is estimated to be $E_{\text{th}} = 1.0f^{1/2} \times 10^{51}$ erg, consistent with the theoretically predicted energy released by a single SN, assuming that the filling factor is unity.

However, the thermal energies of X-ray emitting SNRs have never reached these values, instead being typically $\sim 10^{50}$ erg, as is the case of G 359.77–0.09 and G 359.79–0.26. This inconsistency would be caused by the partial energy transfer from a single supernova explosion to X-rays. The thermal energy of G 359.77–0.09 and G 359.79–0.26 amounts to 3.6×10^{50} erg, if both plasmas have a filling factor of unity. Assuming that the energy contribution of the ring region except for G 359.77–0.09 and G 359.79–0.26 is negligible, the lower limit of the filling factor of the GC ring is estimated to be $f \sim 0.6$. If the filling factor is relatively large, i.e., $f > 0.6$, an additional energy source would be needed. Therefore, we can regard this elliptical arc-like structure as a super bubble, or no less than 2 SNe events.

This putative GC SB has a higher temperature (~ 0.9 keV) than those of the other SBs. We summarize the physical properties of the known Galactic SB candidates in table 3. All the Galactic SB candidates, except for the GC SB, show thermal emission with a temperature of ≤ 0.3 keV. For the extragalactic SBs, Cooper et al. (2004) reported that the diffuse X-ray emission from DEM L192, a SB hosting two OB associations in the LMC, is dominated by a thermal component with the temperature of ~ 0.2 keV. Although 30 Doradus, another SB in the LMC, shows a hard tail, the integrated diffuse emission is fitted by a single-temperature plasma of $kT_e \sim 0.3$ keV (Dennerl et al. 2001; Townsley et al. 2006). Thus the high plasma temperature of the GC SB is unusual.

Furthermore, the plasma density of the GC SB is at least 10 times larger than those of the other SB candidates. Whether the high temperature and the large density are related to some environmental factors peculiar to the GC is an open question. The high temperature of the plasma may also imply hidden non-thermal components or something else.

Some Galactic SBs are known to be related to OB associations. Orion-Eridanus SB is possibly originated from the Orion OB1 association and a following SN explosion with an age of $\sim 1.2 \times 10^5$ yr (Guo et al. 1995). Cygnus SB and the North Polar Spur may obtain their thermal energy from the Cyg OB2 association (Uyaniker et al. 2001) and the Sco-Cen OB association (Egger & Aschenbach 1995), respectively. Thus, we investigated the presence of the OB associations in the GC, using two catalogs of X-ray point sources towards the GC, the Chandra Galactic Center Point Source Catalog (abbreviated to changalcen; Munro et al. 2003) and the Chandra Galactic Central 150 Parsecs Source Catalog (abbreviated to chanc150pc; Munro et al. 2006). We applied both hardness and flux selection to the sources, and found that ~ 50 sources are located within the GC SB. However, all the sources are not brighter than 10^{34} erg s^{-1} in the 0.5–8.0 keV band, when we assume the spectral model and the source distance to be an absorbed power-law ($N_{\text{H}} = 6.0 \times 10^{22}$ cm^{-2} and $\Gamma = 1.7$) and a distance of 8.5 kpc. This examination is consistent with the fact that no candidate of the OB association has been reported in the GC. Hence, it is plausible that the GC SB is formed by multiple (no less than 2) SN explosions.

For the future, a deep X-ray survey in the GC would be required not only to detect the OB association but also to search other SB candidates which may be hidden in the GC.

5. Summary

We summarize the results derived from the G 359.77–0.09 and GC-ring analyses below:

1. The X-ray spectrum of G 359.77–0.09 is well fitted by a thin thermal plasma with a temperature of ~ 0.7 keV. The large absorption towards the plasma ($N_{\text{H}} = 6.9 \times 10^{22}$ cm^{-2}) indicates that the plasma is located in the GC. Since the elemental abundances of Si, S, and Ar are consistent with the solar values, the X-ray emitting plasma is possibly originated from a shock-heated ISM.
2. The radial surface brightness profile constructed from the $K\alpha$ -line band image of He-like sulfur indicates the presence of a large ($20' \times 16'$) ring-like object, which connects two bright X-ray clumps, G 359.77–0.09 and G 359.76–0.26. The absorption column densities of these clumps show the N_{H} dependence on the Galactic latitude near the GC. Furthermore, the X-ray spectrum of the ring-like structure shows the presence of a thin thermal plasma. The thermal energy of the plasma is estimated to be 1.0×10^{51} erg, which exceeds that released by a single X-ray detected SNR. Hence, we propose that the ring-like structure is a super bubble candidate in the GC.

We are grateful to an anonymous referee for his/her fruitful comments and suggestions to improve our paper. We also would like to thank all the Suzaku team members for their support of the observation and useful information on the XIS calibration. N.M. is supported by JSPS Research Fellowship for Young Scientists. This work was supported by the Grant-in-Aid for the Global COE Program "The Next Generation of Physics, Spun from Universality and Emergence" from the Ministry of Education, Culture, Sports, Science and Technology (MEXT) of Japan.

References

- Balucinska-Church, M., & McCammon, D. 1992, *ApJ*, 400, 699
 Bamba, A., Ueno, M., Nakajima, H., & Koyama, K. 2004, *ApJ*, 602, 257
 Bautz, M. W., Kissel, S. E., Prigozhin, G. Y., LaMarr, B., Burke, B. E., & Gregory, J. A. 2004, *Proc. SPIE*, 5501, 111
 Cash, W., Charles, P., Bowyer, S., Walter, F., Garmire, G., & Riegler, G. 1980, *ApJL*, 238, L71
 Cooper, R. L., Guerrero, M. A., Chu, Y.-H., Chen, C.-H. R., & Dunne, B. C. 2004, *ApJ*, 605, 751
 Dennerl, K., et al. 2001, *A&A*, 365, L202
 Dunne, B. C., Points, S. D., & Chu, Y.-H. 2001, *ApJS*, 136, 119
 Egger, R. J., & Aschenbach, B. 1995, *A&A*, 294, L25
 Guo, Z., Burrows, D. N., Sanders, W. T., Snowden, S. L., & Penprase, B. E. 1995, *ApJ*, 453, 256
 Ishisaki, Y., et al. 2007, *PASJ*, 59, 113
 Koyama, K., Awaki, H., Kunieda, H., Takano, S., & Tawara, Y. 1989, *Nature*, 339, 603

Table 3. Properties of the Galactic SB candidates

Name	Distance (pc)	Spatial size	Temperature (keV)	Density (cm^{-3})	References [‡]
Orion-Eridanus SB	226	$20^\circ \times 35^\circ$	0.09–0.15	0.015	1
Cygnus SB	2000	$18^\circ \times 13^\circ$	0.14–0.21	0.02	2,3
Gemini-Monoceros SB	100–1300	$25^\circ \times 25^\circ$	0.08–0.19	0.02–0.05*	4
North Polar Spur	100–210	$34^\circ \times 34^\circ$ [†]	0.17–0.30	~ 0.03	5,6,7
GC SB	8500	$20' \times 16'$	0.91	0.26	our work

* The distance is assumed to be 300 pc.

[†] A spherical shocked plasma with a radius of 140 pc is assumed to be at a distance of 210 pc. The apparent size is $(\Delta l, \Delta b) \sim (15^\circ, 40^\circ)$, based on the ROSAT 3/4 keV map.

[‡] (1) Guo et al. (1995), (2) Cash et al. (1980), (3) Uyaniker et al. (2001), (4) Plucinsky et al. (1996), (5) Egger & Aschenbach (1995), (6) Willingale et al. (2003), (7) Miller et al. (2008)

- Koyama, K., et al. 2007a, PASJ, 59, 23
 Koyama, K., Uchiyama, H., Hyodo, Y., Matsumoto, H., Tsuru, T. G., Ozaki, M., Maeda, Y., & Murakami, H. 2007, PASJ, 59, 237
 Koyama, K., et al. 2007b, PASJ, 59, 245
 Maeda, Y., et al. 2002, ApJ, 570, 671
 Miller, E. D., et al. 2008, PASJ, 60, 95
 Mitsuda, K., et al. 2007, PASJ, 59, 1
 Mori, H., Tsuru, T. G., Hyodo, Y., Koyama, K., & Senda, A. 2008, PASJ, 60, 183
 Munro, M. P., et al. 2003, ApJ, 589, 225
 Munro, M. P., Bauer, F. E., Bandyopadhyay, R. M., & Wang, Q. D. 2006, ApJS, 165, 173
 Nakajima, H., et al. 2008, PASJ, 60, 1
 Nazé, Y., Antokhin, I. I., Rauw, G., Chu, Y.-H., Gosset, E., & Vreux, J.-M. 2004, A&A, 418, 841
 Plucinsky, P. P., Snowden, S. L., Aschenbach, B., Egger, R., Edgar, R. J., & McCammon, D. 1996, ApJ, 463, 224
 Senda, A., Murakami, H., & Koyama, K. 2003, Astronomische Nachrichten Supplement, 324, 151
 Serlemitsos, P. J., et al. 2007, PASJ, 59, 9
 Tawa, N., et al. 2008, PASJ, 60, 11
 Townsley, L. K., Broos, P. S., Feigelson, E. D., Brandl, B. R., Chu, Y.-H., Garmire, G. P., & Pavlov, G. G. 2006, AJ, 131, 2140
 Uchiyama, H., et al. 2007, Proc. SPIE, 6686,
 Uyaniker, B., Fürst, E., Reich, W., Aschenbach, B., & Wielebinski, R. 2001, A&A, 371, 675
 Yamaguchi, H., Bamba, A., & Koyama, K. 2009, PASJ, 61, 175
 Willingale, R., Hands, A. D. P., Warwick, R. S., Snowden, S. L., & Burrows, D. N. 2003, MNRAS, 343, 995